Effect of biaxial Tensile Loading Ratio (σ_x / σ_y) on Stress Distribution Around Crack Tip

Dr. A. K. F. Hassan
Mechanical Engineering Department
College of Engineering
University of Basrah
Basrah - Iraq

Ossama Abdul Aziz
Arabian Gulf Academy
Basrah - Iraq

Abstract

This paper deals with the computer simulation of stress distribution in a plane model of mild steel under biaxial tensile loading. The goal is to visualize the crack behavior under deferent ratios of biaxial loading through linear elastic fracture mechanics theory. A finite element method is considered in calculating the mixed mode of stress intensity factor that governing the influence of stresses distribution around the crack. Aspects of crack propagation are considered. It is found that the maximum circumference stress is not of the plane of crack but that inclined by an angle (68) from it.

تاثير نسبة تحميل الشد باتجاهين (σ_x / σ_y) على توزيع الاجهادات حول مقدمة الشق

د. عبدالكريم فليح حسن
قسم الهندسة الميكانيكية
كلية الهندسة / جامعة البصرة

اسامه عبد العزيز
اكاديمية الخليج العربي للدراسات البحرية
البصرة / العراق

الخلاصة :

يهدف البحث الحالي الى دراسة توزيع الاجهادات حول منطقة الكسر تحت تأثير نسب مختلفة من احمال شد باتجاهين اعتماداً على ميكانيكية الانكسار الخطي المرن. تم اعتماد طريقة العناصر المحددة في حساب معامل شدة الاجهاد لطوري الفتح والقص والذي يعتبر المؤثر المهم الذي يتحكم بتوزيع الاجهادات حول منطقة الكسر. لوحظ ان اقصى قيمة للأجهاد المحيطي ليس في نفس مستوى الكسر بل يميل عنه بزاوية (68).

1. Introduction

Considerable work has already been devoted to study on the crack tip behavior based on uniaxial loading. But the cracked structure may expose to biaxial loading and may have a significant influence on the crack behavior, so these studies do not cover the solution of such problems. However, unexpected results arise like the branched crack propagation, curved crack propagation. Crack closure can be found in structures the subjected to biaxial loading, also, any inclined crack with the axis of uniaxial load, Fig.(1) will be under a mixed mode loading just like the effect of biaxial one. Therefore the real considerable working for the fracture mechanics always takes in account the probability of introduction mixed mode loading. The stress intensity factors are the fundamental quantities describe the stress distribution as a function of crack length and the applied load. These quantities were expressed firstly by

Irwin [1] as a three deferent types of K. The mixed mode of K_I and K_{II} is simulating the crack plane structure. Stress intensity factors used by Paris and Sih [2] to describe the actual displacement at and near a crack. Rice[3] introduce an expression for the J-Integral as an evaluation approach which can be defined as a path independent line integral that measure the strength of singular stress and strain near crack tip.

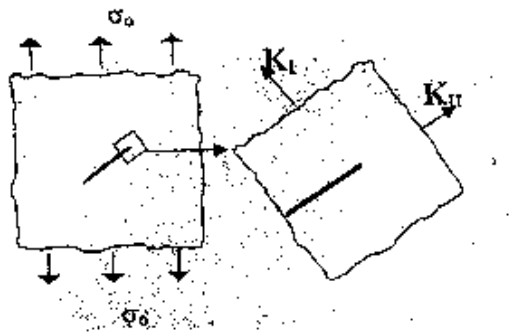

Fig.(1) An inclined crack with the axis of uniaxial load haws mixed mode loading on crack tip.

The basic assumption used, usually, that the crack propagates in a direction that is normal to the maximum tensile stress. The appearance of curved crack, even if it is under uniform tensile loading, supports the theories that state the direction of the next crack tip propagation is not normal to the plane of the load. Tulia[4], proposed that these theories are based on the stress intensity factors and have shown good agreement with experimental results, which represented by Erdogan[5], Hussain[6], and Sih[7]. Erdogan assumes that the crack propagates in the direction that maximizes the function $\sigma(\theta)$, i.e. the circumferential stress around the crack tip. Hussain states that the crack propagates in the direction that maximizes the potential energy released $G(\theta)$, as the crack propagation. While Sih, state that crack extension takes place in the direction along which the strain energy density $S(\theta)$, possesses a minimum value.

2. Theoretical Consideration

2.1 Elastic Finite Element Field Equations

The work is based on the basic principles of linear elastic fracture to solve the stress distribution in the vicinity of crack tip. These stresses will be described by stress intensity factors (SIFs) [1], the ends of a crack in 2D body are called the crack tip, while in 3D stress field the intersection of the crack surface and the body is called crack front, Fig (2). In simulation of crack in 2D plate structure, it is usually the combination of mode I and mode II of SIFs is of interest in this paper.

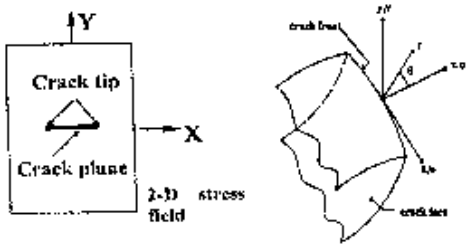

Fig.(2) Crack tip and crack front

Therefore the actual displacement at and near a crack, which can be described as [2]:

$$u = \frac{K_I}{4G}\sqrt{\frac{r}{2\pi}}\left\{(2k-1)\cos\frac{\theta}{2} - \cos\frac{3\theta}{2}\right\} - \frac{K_{II}}{4G}\sqrt{\frac{r}{2\pi}}\left\{(2k+3)\sin\frac{\theta}{2} + \sin\frac{3\theta}{2}\right\} \quad (1)$$

$$v = \frac{K_I}{4G}\sqrt{\frac{r}{2\pi}}\left\{(2k-1)\sin\frac{\theta}{2} - \sin\frac{3\theta}{2}\right\} - \frac{K_{II}}{4G}\sqrt{\frac{r}{2\pi}}\left\{(2k+3)\cos\frac{\theta}{2} + \cos\frac{3\theta}{2}\right\} \quad (2)$$

Where, u and v are the displacements in a local Cartesian coordinate system. r, θ are coordinates in a local cylindrical coordinate system, G is the shear modulus. k= (3-4v) for plane strain or axisymmetric. k= (3-v/1+v) for plane stress. v is the Poisson's ratio. Evaluating Eq.(1) and (2) at θ=± 180 and dropping the higher order terms yield.

$$u = \frac{K_{II}}{4G}\sqrt{\frac{r}{2\pi}}(1+k) \quad (3)$$

$$v = \frac{K_I}{4G}\sqrt{\frac{r}{2\pi}}(1+k) \quad (4)$$

For model symmetric about the crack plane (half-crack model) as shown in Fig.(3-a), Eqs (3) and (4) can be reorganized to give.

$$K_I = \sqrt{2\pi}\,\frac{2G}{1+k}\cdot\frac{|v|}{\sqrt{r}} \quad (5)$$

$$K_{II} = \sqrt{2\pi}\,\frac{2G}{1+k}\cdot\frac{|u|}{\sqrt{r}} \quad (6)$$

For the case of no symmetry (full-crack model) as shown in Fig.(3-b) K_I and K_{II} can be written as:

$$K_I = \sqrt{2\pi}\,\frac{G}{1+k}\cdot\frac{|\Delta v|}{\sqrt{r}} \quad (7)$$

$$K_{II} = \sqrt{2\pi}\,\frac{G}{1+k}\cdot\frac{|\Delta u|}{\sqrt{r}} \quad (8)$$

Where Δv and Δu are the motions of one crack face with respect to the other.

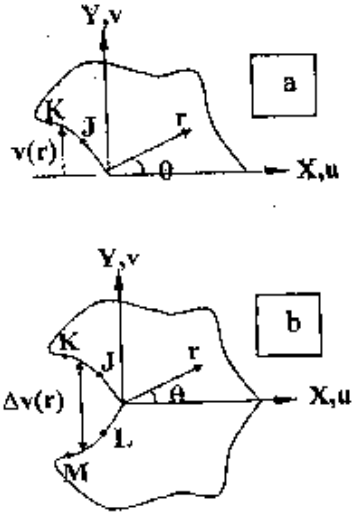

Fig.(3) nodes used for the approximate crack tip displacement: (a) half crack model, (b) full crack model.

2.2 Computation of Stress Intensity Factors (SIFs)

The stress intensity factors are the fundamental quantities describing the singular elastic stresses. They are functions of the length and orientation of the crack, the geometry of the body, and the applied load distribution. A major advance was made by Irwin [1] when he developed the stress intensity approach. From linear elastic theory Irwin showed that the stresses in the vicinity of a crack tip take the from

$$\sigma_{ij} = \frac{K}{\sqrt{2\pi r}} f_{ij}(\theta) \quad (9)$$

Where r, θ are the cylindrical polar coordinates of a point with respect to the crack tip, Fig. (4). K is a

constant called the stress intensity factor, which give the magnitude of the elastic stress filed. The Griffith-Irwin solution for cracked plate gave a more general approach of Eq. (9) to determine the SIF at the tip as

$$K_I = \sigma_o\sqrt{\pi a} \qquad (10)$$

K_I is the opening mode of the stress intensity factor; therefore it can be defined as [8]

$$K_I = \lim_{r\to 0} \sigma_{o(r,\theta=0)}\sqrt{\pi a} \quad (Mpa\sqrt{a}) \qquad (11)$$

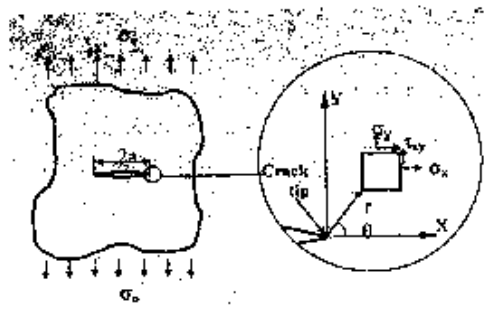

Fig.(4) Crack in finite plate under uniaxial stress.

The stress intensity factors are function of the length and orientation of the crack, the geometry of the body, and the applied load distribution. For the uniaxially loaded case the mode I stress intensity factors can be calculated theoretically from

$$K_I = C\sigma\sqrt{\pi a} \qquad (12)$$

Where, C takes into account the effects of geometry, the crack length and the applied load. C is equal to 1.0 for a crack, located in a uniformly loaded infinite plate perpendicular to the loading direction. Analytical and empirical expressions for stress intensity factors are collected in compendiums such as Tada et al [9] for specimens of simple geometry with various crack configurations and load combinations.

2.3 The J-Integral Evaluation Approach

In its simplest from, the J-Integral can be defined as a path-Independent line integral that measures the strength of the singular stresses and strains near a crack tip. An expression for J in 2D from introduction by rice [10] is shown below. It assumes that the crack lies in the global Cartesian x-y plane, with x parallel to the crack, as shown in Fig.(5).

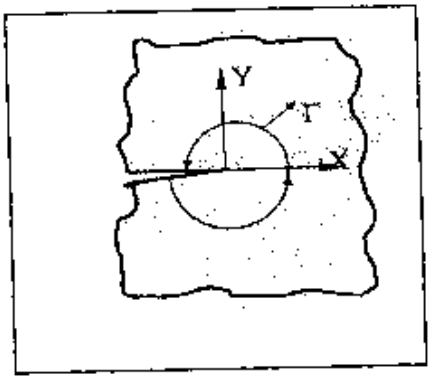

Fig.(5) J-Integral contour path surrounding a crack tip

$$J = \int_{\Gamma} \omega dy - \int_{\Gamma} \underline{T}\frac{\partial \underline{u}}{\partial x} ds \qquad (13)$$

Where Γ is any path surrounding the crack tip, ω is strain energy density (that is, strain energy per unit volume), $\underline{T}$ is traction vector, $\underline{u}$ is traction displacement. To evaluate the stress intensity factor for plane stress the following equation can be written as

$$K_I = \sqrt{JE} \quad for\ plane\ stress \qquad (14)$$

Where, E is the Young modulus. In case of biaxial loading, Irwin[11] used the stress σ_{xx} and σ_{yy} and τ_{xy} to introduce the stress intensity factors as:

$$\begin{Bmatrix} K_I \\ K_{II} \\ K_{III} \end{Bmatrix} = \lim_{r\to 0\ \theta\to 0} \sqrt{2\pi r} \begin{Bmatrix} \sigma_{yy} \\ \tau_{xy} \\ \tau_{yz} \end{Bmatrix} \qquad (15)$$

2.4 The J-angle of maximum stress

In this study, it is demonstrated that the maximum stress, under biaxial tensile loading, occurs at an angle $\theta \neq 0°$. After developing equation. (15), linear elastic approach can be used to predict the direction of the next crack increment, Saouma[12]. Stress intensity factor at each location of the crack tip can be used to deduce the stress concentration. It is necessary to know that this procedure involved remeshing of the domain containing the continuously changing crack geometry and a model for predication of the crack growth. The procedure is agreed with the maximum circumferential stress criterion. Under general mixed mode loading, the asymptotic near-tip circumferential and shear stresses take the form:

$$\begin{Bmatrix} \sigma_{\theta\theta} \\ \tau_{r\theta} \end{Bmatrix} = \frac{K_I}{\sqrt{2\pi r}} \frac{1}{4} \begin{Bmatrix} 3\cos\frac{\theta}{2} + \cos\frac{3\theta}{2} \\ \sin\frac{\theta}{2} + \sin\frac{3\theta}{2} \end{Bmatrix} + \frac{K_{II}}{\sqrt{2\pi r}} \frac{1}{4} \begin{Bmatrix} -3\sin\frac{\theta}{2} - 3\sin\frac{3\theta}{2} \\ \cos\frac{\theta}{2} + 3\cos\frac{3\theta}{2} \end{Bmatrix} \qquad (16)$$

The circumferential stress on the direction of crack propagation is a principal stress. Therefore, the critical angle – defining the radial direction of propagation can be determined by setting the shear stress in Eq. (16) to zero. After a few manipulations, the following expression is obtained:

$$\frac{1}{\sqrt{2\pi r}} \cos\frac{\theta}{2} \left[\frac{1}{2} K_I \sin\theta + \frac{1}{2} K_{II} (3\cos\theta - 1) \right] = 0 \qquad (17)$$

This leads to the equation defining the angle of crack propagation in the tip coordinate system.

$$K_I \sin\theta_c + K_{II} (3\cos\theta_c - 1) = 0 \qquad (18)$$

2.5 The crack tip element

2D quadratic solid elements, area element with a maximum order of eight nodes, Fig.(6), each node has two degree of freedom, this element as a plane element (plan stress) is used in this study, which can represent a finite element model under pressure loading. The specialist of the crack tip element is achieved by placing triangular elements instead of the quadratic one with mid-side node near the crack tip, which obtained by collapsing one side of the quadrilateral element [14], in order to generate only the hard points in the models, where the stress concentration supposed to be, like the crack tip, Fig.(6).

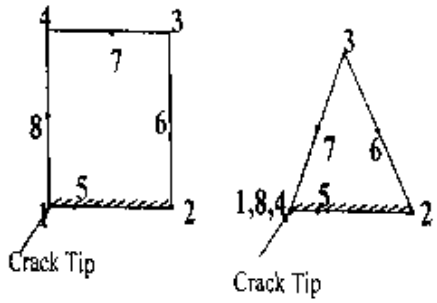

Fig.(6) Singular quadrilateral element for crack tip, with the triangular collapsed element.

Thus, the triangular collapsed elements are chosen in this study to generate only the hard point in the models, where the stress concentrations supposed to be, like the crack tip. Fig.(7) clears the above description and may represent the best refining and orientation of finite element for such single edge cracked plate without symmetry. There is row of 16 triangular elements around the tip, forming a circle with radius of 0.15 a, also the second row around the crack tip will have the same ratio of the first row radius, but with no more triangular elements.

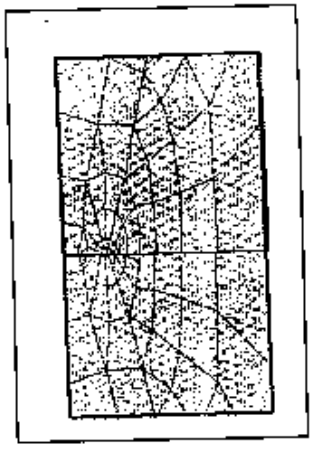

Fig.(7) The finite element mesh used for plate with single edge crack

3. Results and Discussion

The ANSYS finite element package was used to present the stresses distribution in the vicinity of crack tip which may use to describe the crack behavior under different biaxial loading ratios for an isotropic material. The maximum values of these stresses are of most interest to estimate the next propagation of the crack. The model used in this study is a plate with central crack. The material and geometric properties were described in Fig.(8). While the element type is a plane quadrilateral structure solid, has eight nodes with two degree of freedom at each node as shown in Fig.(6).

Five biaxial tensile loading ratios (σ_x/σ_y) in addition to uniaxial one are used to study the biaxiality effect on crack behavior. The loading ratios (0, 0.5, 1., 1.5, 2 and 3) had been chosen. Stress distributions for these cases as a function of the distance from the crack tip were downloaded in only two figures, see Figs.(9) and (10), one figure for Y-direction and the other for x-direction respectively. Fig (9) shows identical distribution of stresses when the loading ratios are $\sigma_x/\sigma_y \leq 1.5$. But there is a sudden drooping of normal stress σ_{yy} at the tip under the biaxiality ratio $\sigma_x/\sigma_y \leq 2$, which can be estimated clearly from Fig.(10) as a variation of stress viruses loading ratio at the tip. It is found that the final identification of stress distributions occurs at the biaxial ratio of $\sigma_x/\sigma_y=1.98$, then the drooping of stress σ_{yy} at the tip from

13.8 σ_y to 7.8σ_y occurs directly before the loading ratio σ_{xx}/σ_{yy}=2.

Fig.(11) describes σ_{xx} distribution under different biaxial loading. It shows that a graduate increment of 0.5σ_y approximately for every 0.5 increment in σ_x/σ_y at the tip. Advancing away from the crack tip, the normal stress σ_{xx} obeyed only the applied stress σ_x. The probability of branched crack propagation or curved crack make all area around crack tip to be investigated, it was found that the circumference stress method is the best one to study the stress distribution and to cover the unexpected results. The area can be divide by similar paths with 15° of deviation between each other with the tip as a center for paths, and three centralized circles are considered with the same tip as a center for them also, the first circle is of 0.1w radius, the second of 0.2w and the third one of 0.5w, where 2w is the width of plate. Due to symmetry only the 1st quarter of the paths and circles plane was considered, Fig.(12) i.e. seven angles (0,15,30,45,60,75,90 degrees) assumed to be related with this work. The results are defined for the points of intersecting between the radial and the three circles (circumferences). It is clear that there is a coincidence of these points on retarding to the tip, so the abundance number of readings is at the neighborhood of crack tip, which represent the most important zone in the area. The intersection of the 1st quarter of circumference with the seven radial paths can be shown in Fig.(13), which represents the variation of stress σ_{yy} in the 1st circumference, with radius of 0.1w, for the three cases of biaxial loading ratio, 0.5, 1, and 1.5 in addition to the uniaxial one. The magnitude of σ_{yy} stress decreased upon increasing the biaxial ratio, but it can be note that for $\sigma_x/\sigma_y \leq 1$, there are some raises in the curves between angles 45° and 75°, which mean that if there is any activity on the crack, it will be in that domain.

In Fig.(14), the σ_{yy} stresses having fewer magnitudes than those of Fig.(13). On advancing away from the hole, at 0.5w, as in Fig.(15) there is less difference in magnitudes between the four distributions along circumference and shows approach with the applied one.

Figs.(13) to (15) show that there is no effect of biaxial loading on the considered area, except the stress increment of distribution between the angles 60° and 90°. To find the exact angle of maximum stress, a refining of the circumference paths between these angles remarked the angle 68°, which define the direction of the assumed crack propagation, as shown in Fig.(16). It is interesting to note that the weakest crack is not the crack normal to the load but the crack inclined at 68° to the load. This is unexpected result. For such model, it is found that the distributions of stresses at x-direction have less respond to the ratio of biaxiality loading than of y-direction. The contour plot of the stress distribution for the central cracked model at the ratio σ_x/σ_y =2

is the represented in Fig.(17). Clearly, the great concentration of stresses at the crack tip reduced at this ratio from 138Mpa to 87.7Mpa, but it still gives the tendency to propagate the crack. The orientation of colors in the plots supports the result of the direction of maximum normal stresses that supposed to be on the path of angle 68° from the crack axis.

4. Conclusions

1. It is found that the stress distribution around the tip of cracked plate, with L=2W, does not change under biaxial loading ratios $\sigma_x/\sigma_y \leq 1.98$, where L and W are the length and width of plate respectively then a large variation occurs directly after this loading ratio.
2. The distribution of normal stress in the x-direction (σ_{xx}) at the crack tip shows a graduate increment of $0.5\sigma_y$ approximately for every 0.5 increment in the biaxial ratio (σ_x/σ_y). But when advancing away from the crack tip, σ_{xx} will reduce only to the value of the applied stress σ_x.
3. The stress distribution along the circumference around crack tip is not uniform. It is found, for such mode for example, that when the applied load is perpendicular to the crack plane, the maximum circumference stress will be at 68°, measured from crack plane. This behavior explains the phenomena of crack curvature in several materials.

References

[1].Irwin G.R. "Analysis of stresses and strains near the end of a crack traversing a plate" , Trans. A.S.M.E., J. Apple. Mech. , 1957.

[2]. P.C. Paris and G.C. Sih, "stress analysis of crack, "ASTM STP 301, 1965.

[3]. Rice, J. R. and Rosengren, G. F., "plane strain deformation near a crack for a power-Law hardening material" J. Mech. Phys. Solids., 16, 1968.

[4]. Tulio N. B. "computer simulation of linear and nonlinear crack propagation in cementitious material" Ph.D. thesis, graduate school of cornell university, 1998.

[5]. Erdogan, F. and Sih, "on the crack extension in plates under plane loading and transverse shear," A.S.M.E. J. of Basic engineering, Vol. 85,pp. 519-527, 1963.

[6]. Hussain M. A., Pu, S. L. and UnderWood J. H., "strain energy release rate for crack under combined mode I and mode II" fracture analysis, ASTM STP 560,pp. 2-28, 1974.

[7]. Sih G. C., "strain-energy-density factor applied to mixed-mode crack problems," Int. J. facture Mech., Vol. 10, pp. 305-321, 1974.

[8]. S. A. Meguid, "engineering facture mechanics" Vol. 37, No. 6, pp. 1251-1275, 1989.

[9]. Tada, H., Paris, P. and Irwin, G. "the stress analysis of cracks handbook" Del research corporation, Hellertown, PA, 1973.

[10]. Rice, J. R. "A path independent integral and the approximate analysis of strain concentration by notches and cracks", J. Mech. Phys. Solids., 16, pp. 1-12, 1968.

[11]. Irwin G. "the crack extension force for a part through crack in plate", transactions ASME, J. Appl. Mech, 1962.

[12]. Victor E. Saouma, "mechanics of materials II" textbook, university of Colorado, Boulder, CO 80309-0428,2002.

[13]. Michael Rye Andersen, "fatigue crack initiation and growth in ship structures" DK-2800 Lyngby, Denmark, ISBM 87-89502-01-9, 1998.

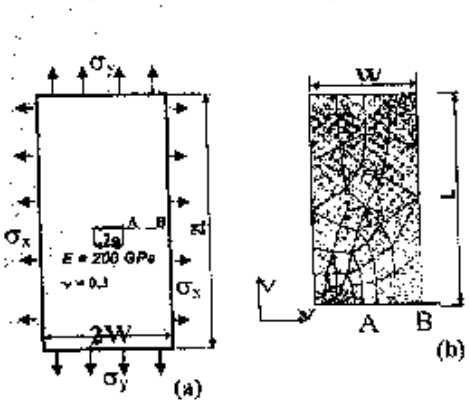

Fig.(8) A plate with central crack under biaxial load
(a) Material properties and geometry.
(b) Finite element model.

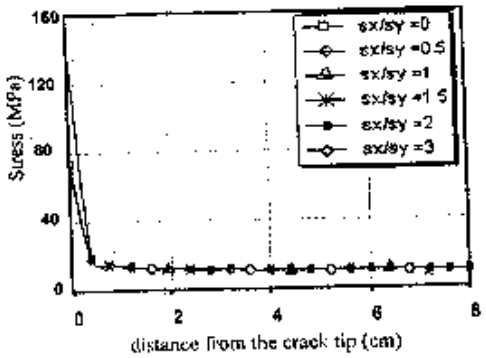

Fig.(9) Variation of σ_{yy} with distance along the path A-B on the central cracked using different biaxial loading.

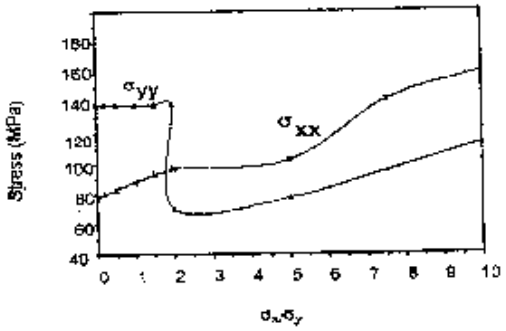

Fig.(10) Variation of σ_{xx} and σ_{yy} at the crack tip with the changing of biaxial tensile load ratio for the cracked model

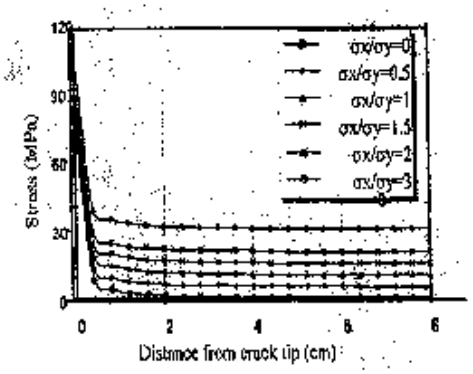

Fig.(11) Variation of σ_{yy} at the crack tip with the changing of biaxial tensile load ratio for the cracked model

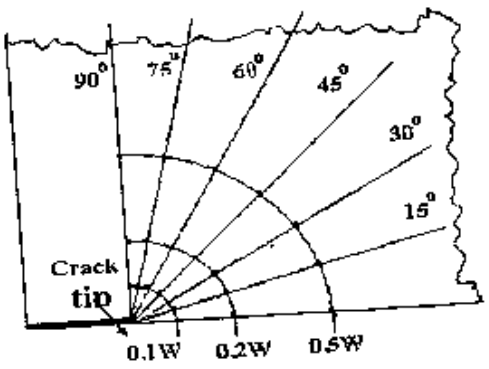

Fig.(12) Dividing the area around crack tip to a radial lines and centralized circles

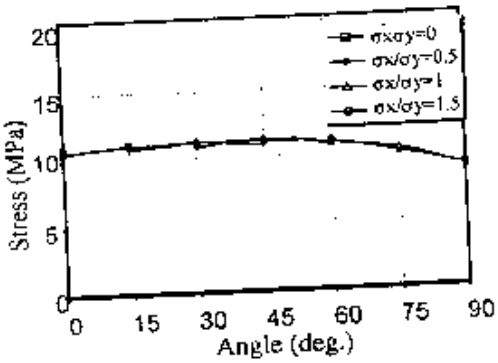

Fig.(15) Fig.(14) Variation of σ_{yy} distribution with angle r=0.5 w from crack tip using different σ_x/σ_y ratios.

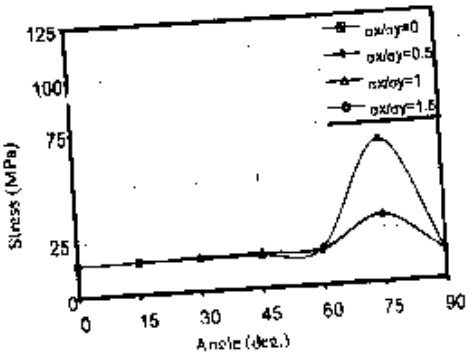

Fig.(13) Variation of σ_{yy} distribution with angle r=0.1 w from crack tip using different σ_x/σ_y ratios.

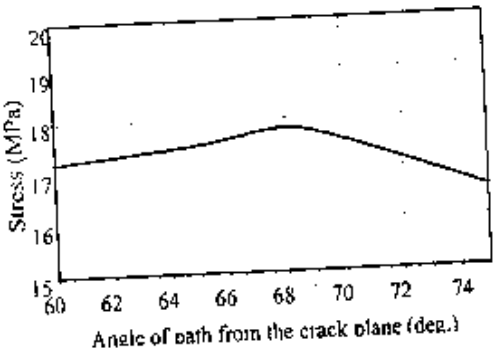

Fig.(16) The angle of maximum σ_{yy} around crack tipat r=0.1 w under uniaxial load

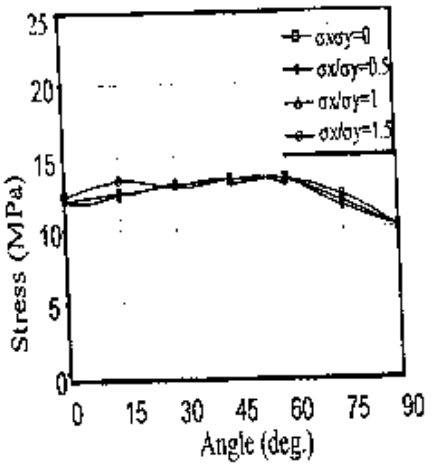

Fig.(14) Variation of σ_{yy} distribution with angle r=0.2 w from crack tip using different σ_x/σ_y ratios.

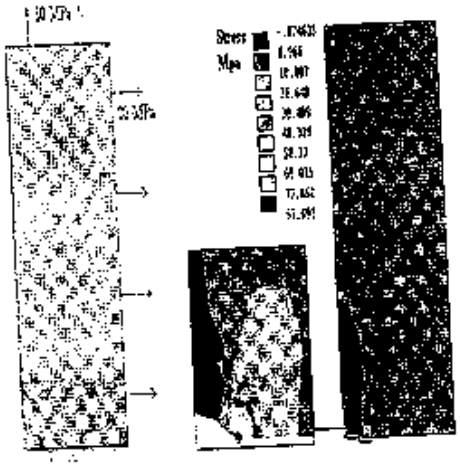

Fig.(17) contour plot of stress for centered cracked plate under biaxial loading ratio $\sigma_x/\sigma_y=2$

A New Hybrid Grid Simulator for Multi Phase Flow in Oil Reservoirs

By
Dr. Ahmed N. Nimir Al-Subeeh
Engineering College – Basrah University

Abstract

In the current study, a new simulator is designed to manipulate what is known as hybrid grid global system for oil reservoir simulation. The global system composed of two subsystems, one covering the regions around the well which is called radial (r-θ) model while the second is linear (x-y) which covers the rest of reservoir regions. The constructed simulator is able to deal linear and radial two phase flow compressible oil water with the consideration of the rock compressibility. The two subsystems are solved simultaneously within the global system of the reservoir. The outer and inner boundary conditions between the two systems are treated and improved interactively during each time step depending on the relative positions of the two subsystems in reservoir. The method of formulation and system solving also are introduced with the main characteristics of the new simulator.

الخلاصة

في الدراسة الحالية، تم تصميم نموذج محاكاة للمكامن النفطية لمعالجة ما يسمى بنظام الشبكة المهجن العام والذي يتكون من نظامين فرعيين احدهما يتعامل مع طبيعة الجريان الشعاعي في المناطق المحيطة بالبئر و بالأبعاد (r-θ) والثاني هو نظام خطي (x-y) والذي يتعامل مع الجريان الخطي في المناطق الأخرى من المكمن. النموذج المقترح قادر على التعامل مع الجريان بطورين للماء و النفط مع اخذ انضغاطية الصخر بعين الاعتبار. يتم حل النظام الخطي و الشعاعي آنيا ضمن النظام العام ويتم معالجة و تحديث الشروط الحدية الخارجية والداخلية بالاعتماد على نتائج كل منهما خلال كل فترة زمنية. و يستعرض البحث طريقة التصميم وصياغة المعادلات لنموذج المحاكاة المقترح في هذه الدراسة.

Introduction

A reservoir simulation study is the most effective means of achieving a global picture of the reservoir system. It can be thought as an effective tool for screening, analysis and design.
Simulator can be regarded as the basic tool to conduct a reservoir simulation study. It requires a good understanding of the physical processes occurring in the reservoirs and a high level sophistication and maturity in advanced mathematics and computer programming. The cornerstones of a reservoir simulation are:

1- The mathematical modeling.
2- Laboratory investigation
3- Field observations.
4- Computer code.

These four cornerstones are interacting with each other such that a continuous feedback tales place for the mutual benefit and enhancement of all the parts.

Even with the continual advances made in both computational algorithms and computer hardware used in reservoir modeling studies, large-scale simulation of fluid and heat flow in heterogeneous reservoirs remains a challenge. The problem commonly arises from intensive computational requirement for detailed modeling investigations of real-world reservoir.[1]

Computational efficiency and memory scalability are the major subjects in large-scale reservoir simulations. [2]

Reservoirs with long producing life are containing the remaining oil in staggered regions, also most reservoirs have sophisticated structure and geological formation. From other hand, the presence of a well in the reservoir led to cylindrical flow and high sensitive regions around the well itself with high rates of change through these regions. For these reasons and others, the conventional simulators are not preferred which require huge input data and may give wrong prediction.

In the current study, a new simulator is designed to study the flow of two phase oil – water in oil reservoir represented by hybrid grid system. The method of formulation and system solving also are discussed with the main characteristics of the new simulator.

Formulation method

Dakuang et. al. [3] 2005, illustrated the important reasons for the requirements of more sophisticated simulators. The long life of reservoir production and the reservoir of mature stage with high water cut and high recovery led to distribute the remaining oil in scattered patterns in the reservoir. These scattered zones are more important than other regions, and thus more focusing are needed in these regions. In other cases, the large-scale sophisticated reservoir requires highly complex data and mathematical efforts.

One of the main important solutions for such cases is to combine coarse grid simulation with fine grid simulation techniques. The underground flow of compressible oil and water through porous media in oil reservoir can be governed by what is known as diffusivity equation. The diffusivity equation can be derived by applying the mass conservation, an equation of state and energy equation. The full derivation can be found in references [4], [5], and [6].

For two dimensional two phase flow of compressible oil and water through a porous media, the diffusivity equations are as follows:

$$\frac{\partial}{\partial x}\left[\lambda_{wx}\left(\frac{\partial P_w}{\partial x}-\gamma_w\frac{\partial h}{\partial x}\right)\right]+\frac{\partial}{\partial y}\left[\lambda_{wy}\left(\frac{\partial P_w}{\partial y}-\gamma_w\frac{\partial h}{\partial y}\right)\right]+\tilde{q}_w=\frac{\partial}{\partial t}\left[\phi S_w b_w\right] \quad \ldots\ldots(1)$$

$$\frac{\partial}{\partial x}\left[\lambda_{ox}\left(\frac{\partial P_o}{\partial x}-\gamma_o\frac{\partial h}{\partial x}\right)\right]+\frac{\partial}{\partial y}\left[\lambda_{oy}\left(\frac{\partial P_o}{\partial y}-\gamma_o\frac{\partial h}{\partial y}\right)\right]+\tilde{q}_o=\frac{\partial}{\partial t}\left[\phi S_o b_o\right] \quad \ldots\ldots(2)$$

Where λ_{WX} and λ_{OX} can be defined as:

$$\lambda_{wx}=\frac{K_x.K_{rw}.b_w}{\mu_w} \quad \ldots\ldots(3)$$

$$\lambda_{ox}=\frac{K_x.K_{ro}.b_o}{\mu_o} \quad \ldots\ldots(4)$$

The compressibility of fluids and formation rocks are considered. Applying the finite difference and discretization methods, eqt.(1) and eqt.(2) can be transformed to the following equations:[4]

$$\Delta_x\left[T_{wx}\left(\Delta_x P_w-\gamma_w\Delta_x D\right)\right]_i^{n+1}+\Delta_y\left[T_{wy}\left(\Delta_y P_w-\gamma_w\Delta_y D\right)\right]_i^{n+1}+Q_{wij}=\frac{V_{bij}}{\Delta t}\Delta_t\left[\phi S_w b_w\right]_{ij} \quad \ldots\ldots(5)$$

$$\Delta_x\left[T_{ox}\left(\Delta_x P_o-\gamma_o\Delta_x D\right)\right]_i^{n+1}+\Delta_y\left[T_{oy}\left(\Delta_y P_o-\gamma_o\Delta_y D\right)\right]_i^{n+1}+Q_{oij}=\frac{V_{bij}}{\Delta t}\Delta_t\left[\phi(1-S_w)b_o\right]_{ij} \quad \ldots\ldots(6)$$

$$T_{wxi+\frac{1}{2}}\left(\Delta_x Pw-\gamma_w\Delta_x D\right)_{i+\frac{1}{2}}^{n+1}=T_{wxi+\frac{1}{2}}\left[\left(Pw_{i+1}-Pw_i\right)-\gamma_{wi+\frac{1}{2}}\left(D_{i+1}-D_i\right)\right]^{n+1} \quad \ldots(7)$$

$$T_{wx(i-\frac{1}{2})}\left(\Delta_x Pw-\gamma_w\Delta_x D\right)^{n+1}_{i-\frac{1}{2}}=T_{wx(i-\frac{1}{2})}\left[\left(Pw_i-Pw_{i-1}\right)-\gamma_{w_{i-\frac{1}{2}}}\left(D_i-D_{i-1}\right)\right]^{n+1} \quad \ldots\ldots(8)$$

Hybrid grid system

Equations (5) and (6) describe the two phase flow through porous media within two linear dimensions (x-y) as shown in Fig.(1).

The production rate ($\tilde{q}_o$) and injection rate ($\tilde{q}_w$) terms in equations (1), (2) and equations (5), (6) are playing as sink or source terms. These terms transform the effects of producing well or injection well to the reservoir. The effects of the sink or source terms are initiated within its containing blocks and then propagate through the remaining reservoir. The rate of propagation depends on many factors such as the magnitude of production or injection rates, the size of well block, the surrounding properties, and the location of block containing the well relative to the boundaries of the reservoir system.

The surrounding area around the well position is of highly importance and sensitivity. This is due to the high rates of change in pressure and fluid saturations occurred around the well. Also, the flow stream in these areas is purely radial and not linear in nature. So, to describe the regions around the well accurately, it is highly recommended to use a governing equation of flow which is different from that used to describe the flow away from the well.

The diffusivity equations describing the flow in radial two phase compressible flow are: [8]

$$\frac{1}{r}\frac{\partial}{\partial r}\left(r.\gamma_o.\frac{\partial\Phi_o}{\partial r}\right)=\frac{\partial}{\partial t}\left(\frac{\phi}{B_o}\right) \quad \ldots.(9)$$

$$\frac{1}{r}\frac{\partial}{\partial r}\left(r.\gamma_w.\frac{\partial\Phi_w}{\partial r}\right)=\frac{\partial}{\partial t}\left(\frac{\phi}{B_w}\right) \quad \ldots(10)$$

To describe the flow around the well, a cylindrical (r-θ) diffusivity equation are required as shown in equation (11) for oil phase and equation (12) for water phase.[8], [9]

$$\frac{1}{r}\frac{\partial}{\partial r}\left(r.\gamma_o.\frac{\partial\Phi_o}{\partial r}\right)+\frac{1}{r^2}\frac{\partial}{\partial\theta}\left(\gamma_o.\frac{\partial\Phi_o}{\partial\theta}\right)=\frac{\partial}{\partial t}\left(\frac{\phi}{B_o}\right)\ldots\ldots\ldots\ldots(11)$$

$$\frac{1}{r}\frac{\partial}{\partial r}\left(r.\gamma_w.\frac{\partial\Phi_w}{\partial r}\right)+\frac{1}{r^2}\frac{\partial}{\partial\theta}\left(\gamma_w.\frac{\partial\Phi_w}{\partial\theta}\right)=\frac{\partial}{\partial t}\left(\frac{\phi}{B_w}\right)\ldots\ldots\ldots\ldots(12)$$

Grid orientation effect and stream lines

The grid orientation effect is along standing problem plaguing reservoir simulation.[10] The existing anisotropy determine the orientation of a coordinate system's principal axes. In most applications, reservoir simulators employ orthogonal coordinate systems, where all the axes are mutually perpendicular. It is imperative to align these axes with the principal flow directions as shown in Fig.(3).

The first step in constructing a numerical model is the placement of the axes. Permeability anisotropy and coordinate orthogonality must be considered to achieve good grid orientation.

A rotation of the computational grids yields a sub standing different solution finite difference schemes.[10]

The grid size and the number of grid blocks are dependent of each other. In a defined fixed reservoir system, specifying the grid size determines the number of grid blocks. The number and positions of wells in the reservoir play a dominate role in grid size and type selection. As mentioned previously, the flow around the well region is radial in nature while the flow in region away from the well is linear. Combining linear and radial grids is the best solution for simulating a reservoir containing wells. The hybrid grid system can be as shown in Fig.(4).

Boundary conditions

As it is well known, the partial differential equations that describe flow in porous media have constraints known as initial and boundary conditions. The resulted mathematical and difference model composed of two types of sub systems, the first subsystem is away from the well is containing the linear flow, and the second subsystem containing the cylindrical flow is around and near the well region. The global grid system contains linear (x-y) grid and cylindrical (r-θ) grid.

Since the radial flow region around the well position is bounded by several blocks, and since these blocks my have different conditions and properties which led to different boundary conditions around the outer boundary or region during different time periods.

The inner boundary conditions between the two subsystems are treated interactively. This is depending on the relative positions of the two subsystems in the global reservoir system. The boundary conditions between the two subsystems coordinate the relation between the two subsystems. For example, considering the system illustrated in Fig. (4), the boundary conditions of the outer region of cylindrical subsystem are determined from the new values of the surrounding blocks in the linear subsystem. These values are improved and corrected continuously during each time period. In the same manner, the boundary conditions for linear subsystem are dynamically determined from the cylindrical subsystem and used automatically to solve the set of linear subsystem equations.

Solution approach

A new simulator is constructed in the current study for hybrid cylindrical (r-θ) – linear (x-y) grid system to simulate the two phase compressible oil – water flow through porous media. The compressibility of formation rocks are considered.

The constructed simulator is able to handle the cylindrical flow nature around and near the well region and solve their system of governing equations with improved boundary conditions separately. The linear (x-y) set of equations are solved with converged results. The simultaneous solution method is used with applying simple iteration method in iteration. At each time step, the effects of producing wells or/and injection wells are transformed to the global system when the solution of cylindrical subsystem is converged. These effects are introduced to global system effect through the improving of boundary conditions and the converged values of cylindrical subsystem. This iteration is continued until convergence is achieved for each time step. The schematic drawing shown in Fig.(5) explains the treatment of the two grid subsystems during one iteration, while Fig.(6) illustrates the solution approach.

Tested Problems

The constructed simulator in this study tested with a number of cases. One of

them is an oil reservoir with two phase flow, oil and water. The extension of this reservoir is about 5600 m in length and the same extension in width which is covering an area about 31360000 square meters. The other important properties are shown in Table (1). The compressibility of oil, water, and formation rock are considered. A coarse linear grid of eight blocks in I direction with eight blocks in J direction. There is one exploration oil producing well at block (I=8, J=1). The block containing a well is treated as a separate cylindrical subsystem to handle the cylindrical (r-θ) flow near and around the well region. The remain global system is considered as linear in two dimension (x-y). The primary producing rates are not exceeding the values beyond which the pressure drawdown exceeds the limits of bubble point pressure. This case is known as case number (1.1) in the current study, and the results of the run are shown in Fig.(7) after 2500 days of simulation, while Fig.(8) shows the result of the run after 5000 days. The numbering scheme is shown in Fig.(9). The results of the cylindrical flow in block (I=8, J=1) for the same time are shown in Table (2) and Table (3)

Fig.(7) illustrates the pressure distribution of oil phase (Po) for the linear subsystem at the end of accumulated time equal to (2500 Day) according to grid of (8x8) blocks and wil production rate equal to (81 STB/Day). The well is situated at block (i=8, j=1). The pressure distribution for radial subsystem is shown in Table(2) which shows four sectors in M direction (j=1 to 4) and nine rings in N direction (i=1 to 9). The first ring (i.e. i=1, j=1,2,3,4) is surrounding the bore hole of the well, while the outer ring of the radial subsystem (i.e. i=9, j=1,2,3,4) is adjacent to the linear subsystem.

It can be seen from Fig. (7) and Table(2) the final oil pressure after 2500 day at the well grid block in the linear subsystem is equal to (3907 Psi). This is the same value which calculated in the radial subsystem of outer ring (i.e. i=9, j=1, 2, 3, 4) as shown in Table (2)

Fig. (8) demonstrates another run for the same case (1.1) but for accumulated run time equal to (5000 Day) and oil production rate equal to (100 STB/Day). Due to higher production rates in the second run, the pressure drawdown is more than that in the first one. The well hole pressure is about (2000 Psi.) (Grid i=1,j=1,2,3,4 in radial subsystem) and the pressure at the outer boundary of radial subsystem is about (3436 Psi.) (grid i=9, j=1,2,3,4)which is the same calculated value in the linear grid (i=8,j=1).

Conclusions

1- The current study introduces a new approach to improve the boundary conditions for the hybrid grid model containing radial and linear subsystems.
2- The simultaneous solution of the radial and linear subsystems in the global model insures more accurate treatment of the boundary conditions.
3- Fluid flow through the reservoir is treated depending on the nature of flow itself and thus gives more accurate handling of fluid flow types.
4- the grid networks in the proposed simulator are designed with consideration of fluid flow type and streamlines of flow which led to minimization of what is known as grid effect on the current simulator.
5- Due to using hybrid grid network, the cells can be fine in the interested area and coarser in the other regions which led to minimization in input data,

elapsed treatment time, and computer requirements.

Nomenclature

A	Cross – sectional area of a block , Sq.ft.
B_l	Formation volume factor of phase l , SCF/cu.ft.
b_l	1/Bl Shrinkage factor of phase l, cu.ft./SCF.
C_f	Formation compressibility, Psi^{-1}.
C_o	Oil compressibility, Psi^{-1}.
C_w	Water compressibility, Psi^{-1}.
D	Depth of grid block from certain datum, ft.
H	Thickness of grid block, ft.
I	Number of grid block in the x-direction.
J	Number of grid block in the y-direction.
Kr_l	Relative permeability of phase l.
Kx	Horizontal absolute permeability in the x- direction, md.
Ky	Horizontal absolute permeability in the y- direction, md
ρ_c	Capillary pressure , Psi.
P_l	Pressure of phase l , Psi.
P_{wf}	Flowing well pressure , Psi.
Q_l	Flow rate of phase l, SCF/D.
q_l	Flow rate of phase l, SCF/D/ cu.ft. of grid bulk volume.
r	External radius of grid block, ft.
re	External radius of aquifer block , ft.
ro	Equivlant radius of well , ft.
R_w	Radius of well, ft.
R_s	Solution gas / oil ration SCF/STB.
S_l	Saturation of phase l. fraction .
T_l	Finite – difference transmissibility for phase l, cu.ft. / (day-Psi).
x,y	Directions in the Cartesian co-ordinate system.

Greek symbols

∇	Differential operator .
Δ	Difference operator .
Δ_s	Grid spacing of co-ordinate s (X,Y), ft.
Δ_x	Horizontal difference operator in the x- direction.
Δ_y	Horizontal difference operator in the y- direction.
γ_l	Density of phase l in terms of gradient, Psi. /ft.
λ_l	Mobility of phase l, md/ c.p.
μ_l	Viscosity of phase l, c.p.
ϕ	Porosity, fraction.
Φ_l	Potential of phase l, Psi.

Subscript Symbols

i	Grid block index in the x-direction.
$i \pm \frac{1}{2}$	Boundary indices of grid block in the x-direction.
j	Grid block index in the y-direction.
$j \pm \frac{1}{2}$	Boundary indices of grid block in the y-direction.
l	Phase , l = o, g, w
g	Gas.
o	Oil.
r	Rock.
w	Water.

Superscript Symbols

n	Time level.
/	Derivative.

References

1- Keni Zhang, Yu-Shu Wu, Chris Ding, and Karsten Pruess, ' Application of Parallel Computing Techniques to a Large-Scale Reservoir Simulation ', Proceeding: Stanford University, SGP-TR-168, 29-11-2001.

2- Cao Jianwen, ' Application of a Parallel Reservoir Simulator to Large-Scale Industrial Test Cases on a Beowulf Cluster ', Parallel Computing Laboratory, CAS, China, 2003.

3- Dakuang Han, Jingrong Wang, and Jigen Ye, ' New Demands for Application of Numerical Simulation to Improve Reservoir Studies in China ', International Journal of Numerical Analysis and Modeling, Vol. 2, Supp, P.: 148-152, 2005.

4- Ahmed N. Nimir Al-Subeeh, ' Sectorial Study of water Front Advancement In North Rumaila oil Field – Main Pay ', Ph. D. Thesis, Petroleum Engineering Department, Engineering College, Baghdad University, Dec.-2000.

5- Ahmed N. Nimir Al-Subeeh, ' Using Triangular Shape Cell in Reservoir Simulation ', Basrah 7th. Scientific Conference for Engineering Researches, engineering College – Basrah University, 19-20 march 2008.

6- Crichlow H. B., ' Modern Reservoir Engineering – A Simulation Approach ', Prentice Hall, Inc., New Jersey, 1997.

7- Geir Terje Eigestad, ' Reservoir Simulation with Imposed Flux Continuity Conditions on Heterogeneous and Anisotropic Media for General Geometries and The Inclusion of Hysteresis in Forward Modeling ', Ph.D. Thesis, Department of Mathematics, University of Bergen, April 2003.

8- Mohammed G. Al-Rubayee, ' Numerical Model for Single Well in Fractured Reservoir, Two-Dimension Radial Flow, Two-Phase Oil and Water ', M. Sc. Thesis, Petroleum Engineering Department, Engineering College, Baghdad University, Dec.-2001.

9- Turgay Ertekin, Jamal H. Abow Kassem, and Gregory R. King, ' Basic Applied Reservoir Simulation ', SPE Inc., 2001.

10- E. Chong, Z. Syihab, E. Putra, D. Hidayati, and D. Schechter, ' A New Grid Block System for Reducing Grid Orientation Effect in Oil Reservoir Simulation Process ', Archives of Mining Sciences Journal, 51-3-2008.

11- Chakib Bennis, ' Hybrid LGR for Accurate Reservoir Flow Simulation ', Tetrahedron Workgroup, INRIA Rocquencourt, France, Oct. – 2007.

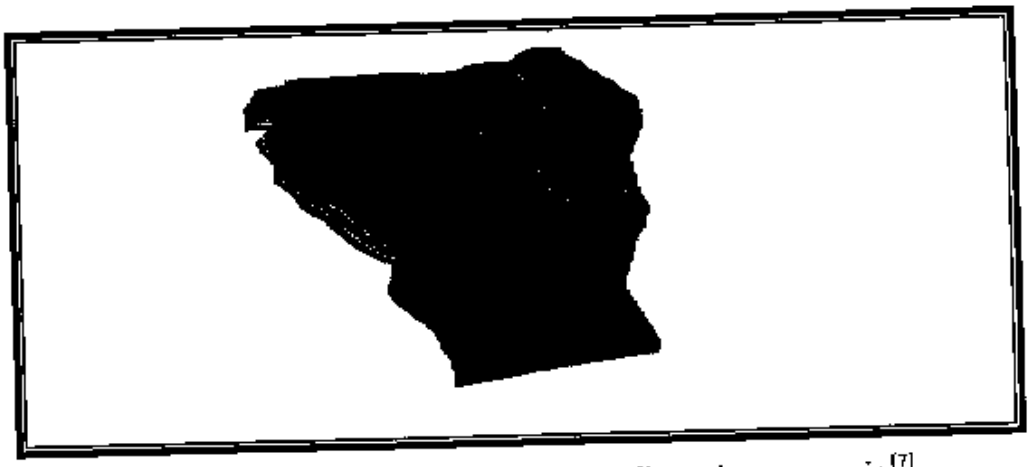

Figure (1) An example of complex two dimensions reservoir.[7]

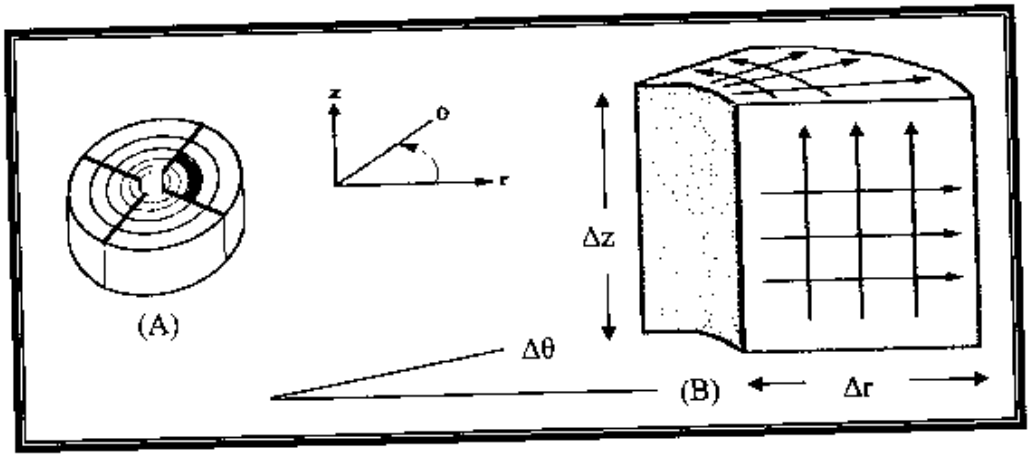

Figure (2) A – Cylindrical grid and B- The element of cylindrical system.

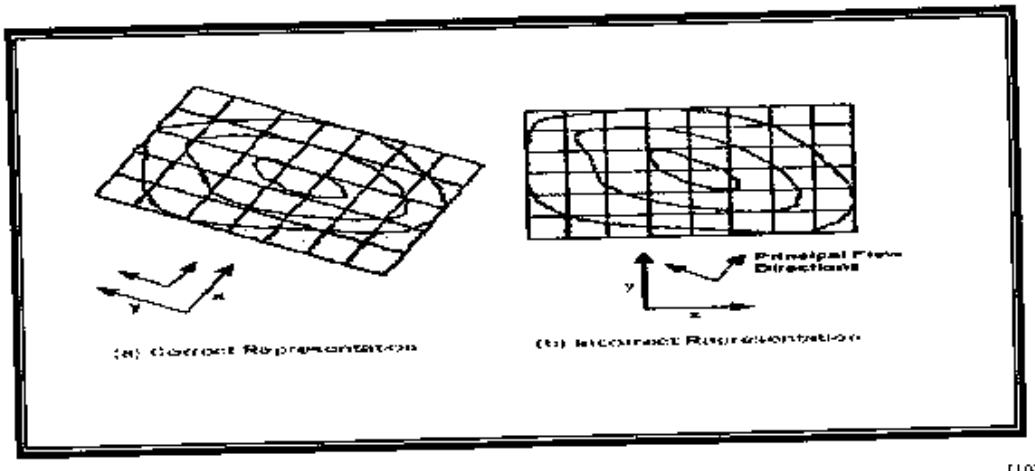

Figure (3) The effect of the grid system orientation with respect to main stream lines.[10]

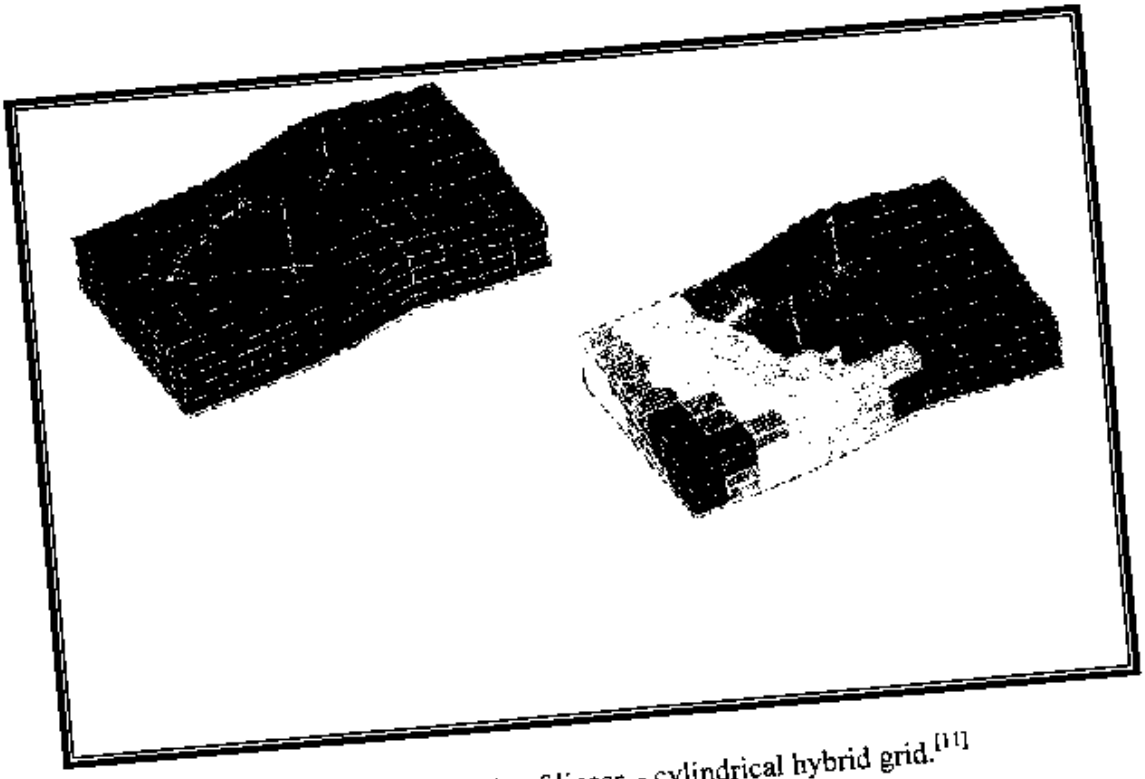

Figure (4) An example of linear – cylindrical hybrid grid.[11]

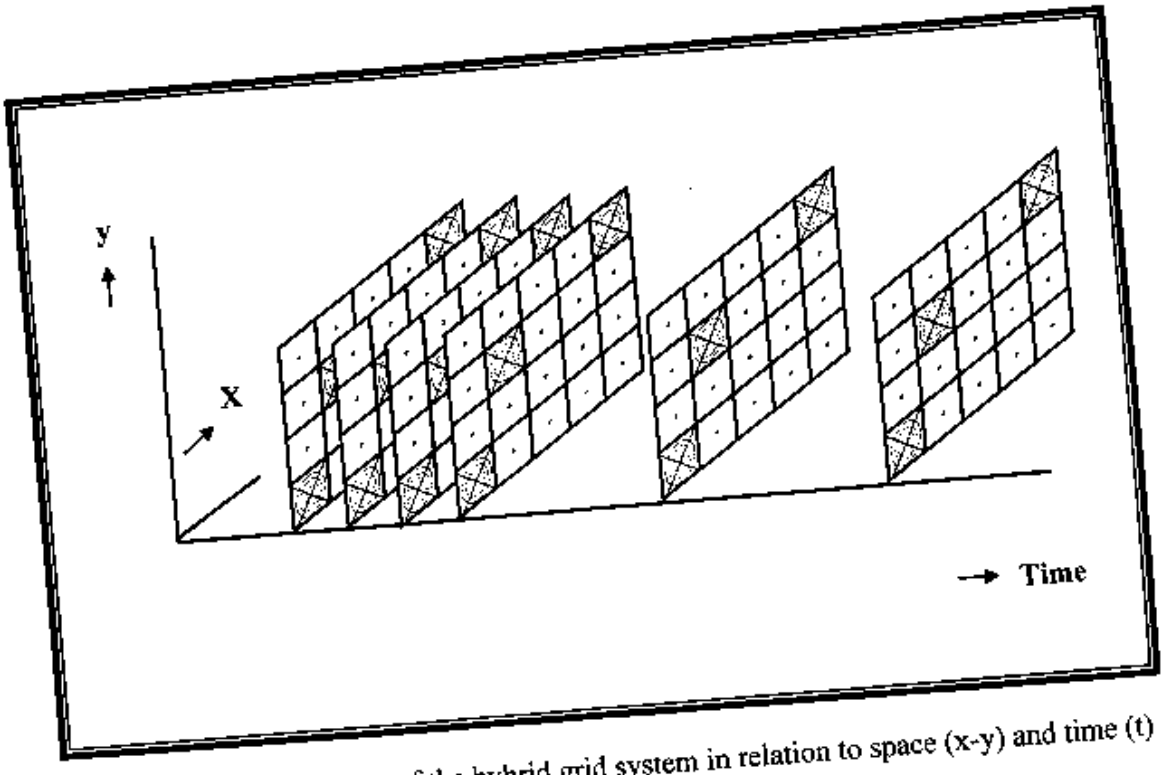

Figure (5) The treatment of the hybrid grid system in relation to space (x-y) and time (t)

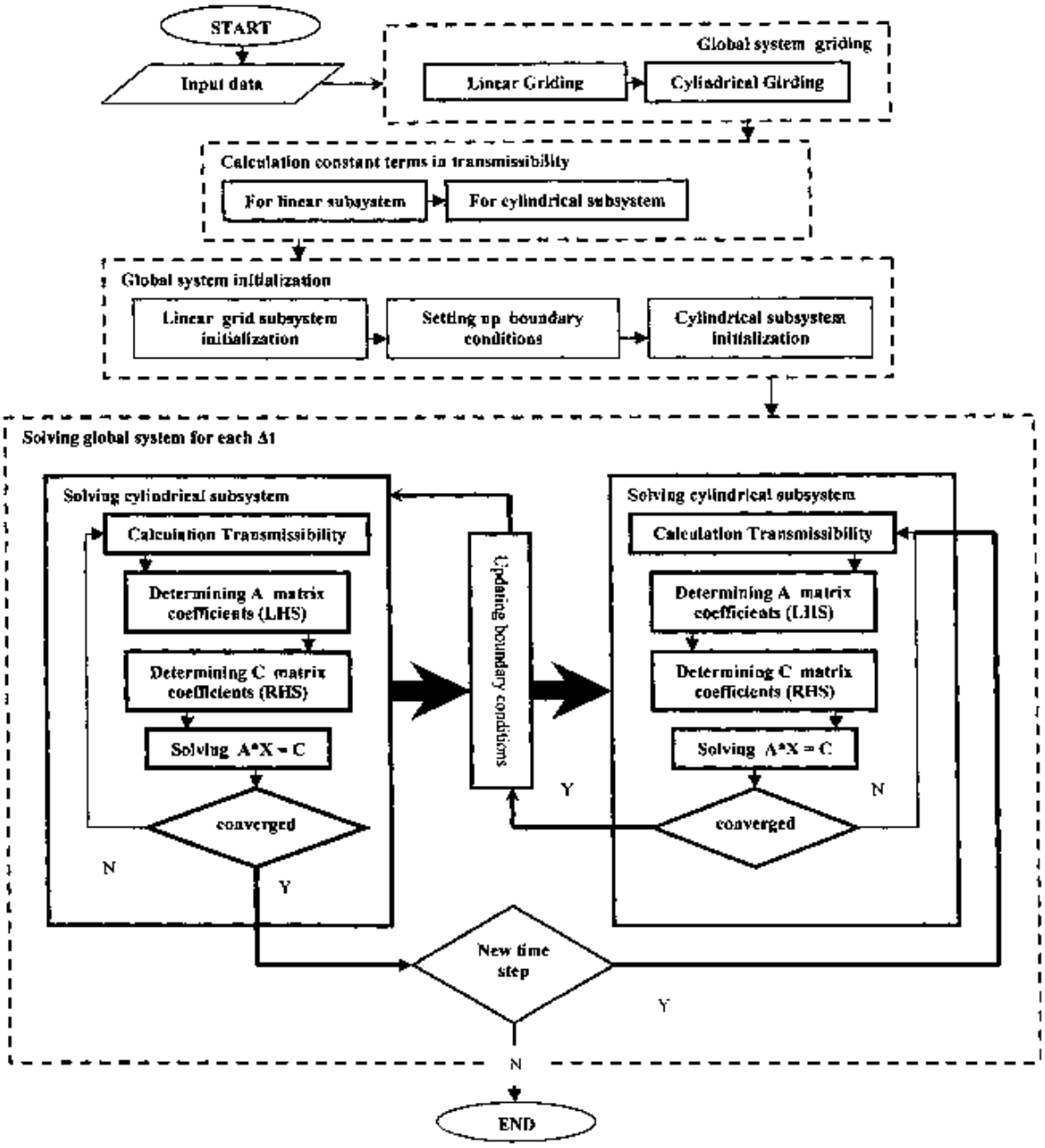

Figure (6) Simple flowchart explains the main processes in the hybrid grid simulator in the current study.

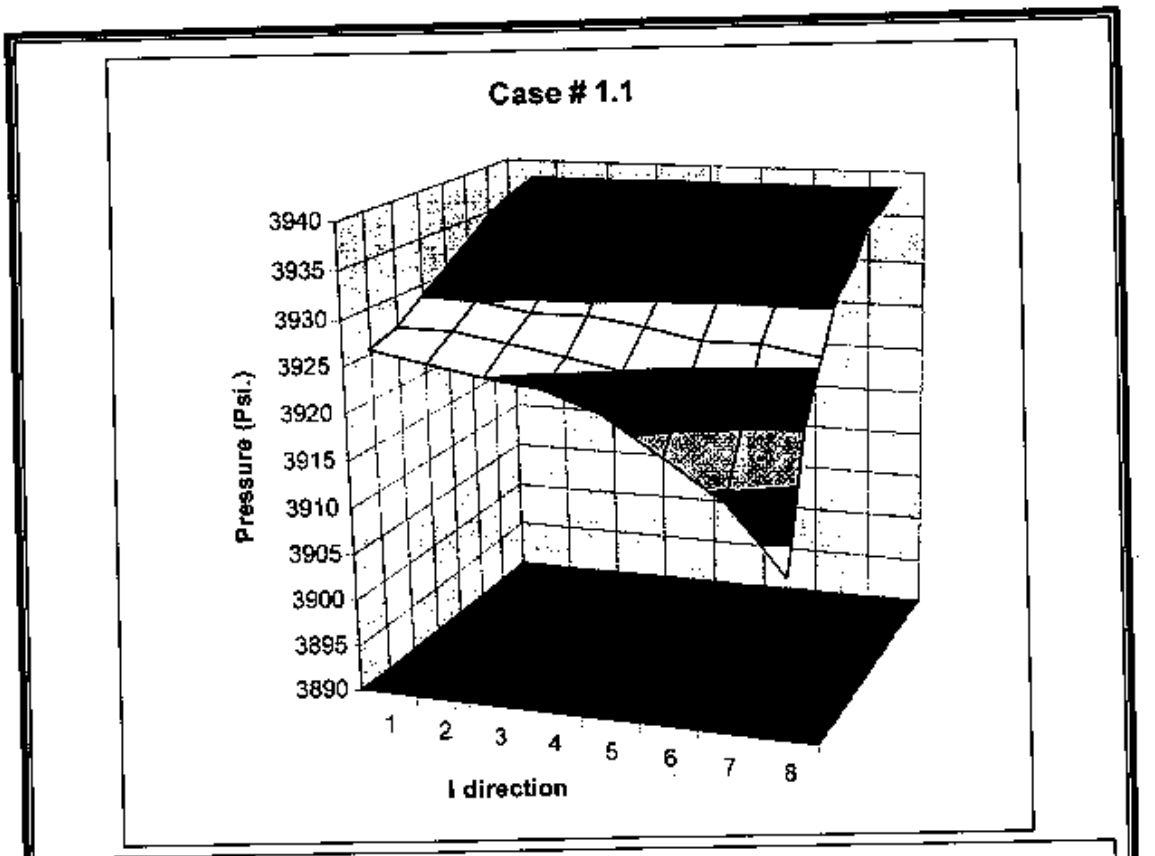


```
*** Elapsed Time =              .34E+05 SEC.
*** DYNAMIC LINEAR
 ACC. TIME =      2500.000 Day.  DT.=       .001000
 Po (Psi.)                 LAYER  1
Acc. Oil Prod.=      .81E+02 Acc. We=       .00E+00   MSTB
```

j \ i	1	2	3	4	5	6	7	8
1	3927	3926	3925	3924	3922	3918	3914	3907
2	3928	3928	3927	3926	3925	3923	3921	3920
3	3930	3930	3929	3929	3928	3927	3927	3926
4	3932	3932	3932	3932	3931	3931	3931	3931
5	3934	3934	3934	3934	3934	3934	3934	3933
6	3936	3936	3936	3936	3936	3936	3936	3936
7	3937	3937	3937	3937	3937	3937	3937	3937
8	3938	3938	3938	3938	3938	3938	3938	3938

Figure (7) Results of case # 1.1 after 2500 days (first run).

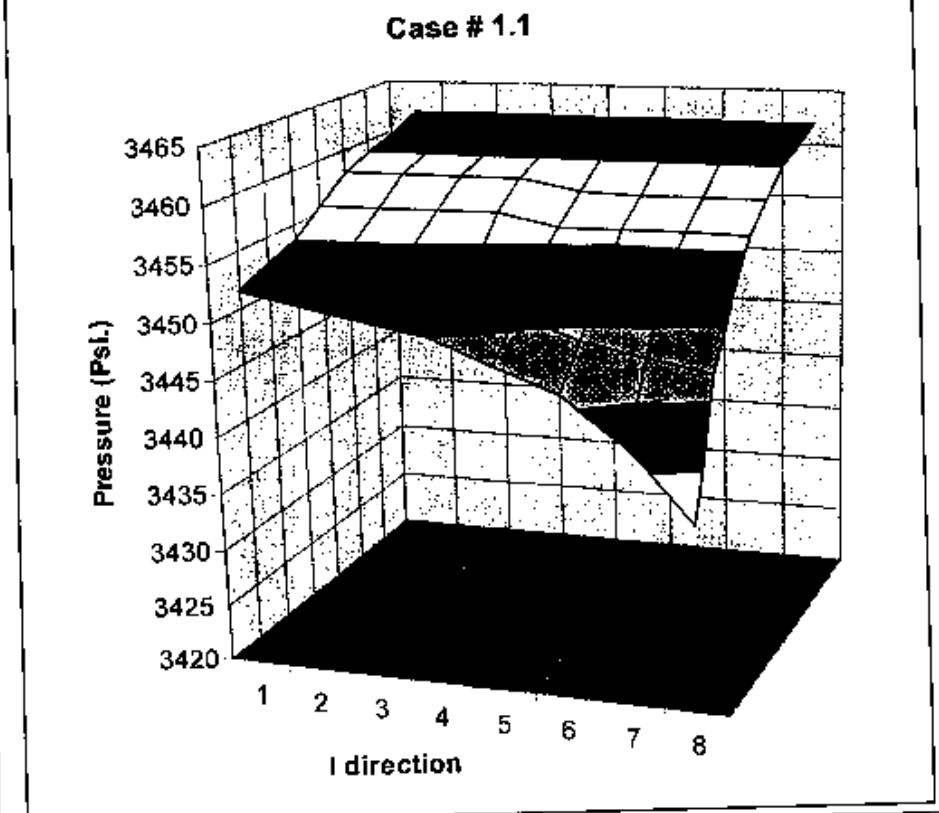


```
 *** Elapsed Time =              .64E+05 SEC.
 *** DYNAMIC LINEAR
ACC. TIME =      5000.000 Day.  DT.=       .000999
Po (Psi.)                LAYER  1

Acc. Oil Prod.=      .10E+03 Acc. We=      .00E+00   MSTB
```

j \ i	1	2	3	4	5	6	7	8
1	3453	3452	3451	3450	3448	3446	3442	3436
2	3454	3453	3453	3452	3451	3449	3448	3447
3	3455	3455	3455	3454	3454	3453	3453	3452
4	3457	3457	3457	3457	3456	3456	3456	3456
5	3459	3459	3459	3459	3458	3458	3458	3458
6	3460	3460	3460	3460	3460	3460	3460	3460
7	3461	3461	3461	3461	3461	3461	3461	3461
8	3462	3462	3462	3462	3462	3462	3462	3462

Figure (8) Results of case # 1.1 after 5000 days (second run).

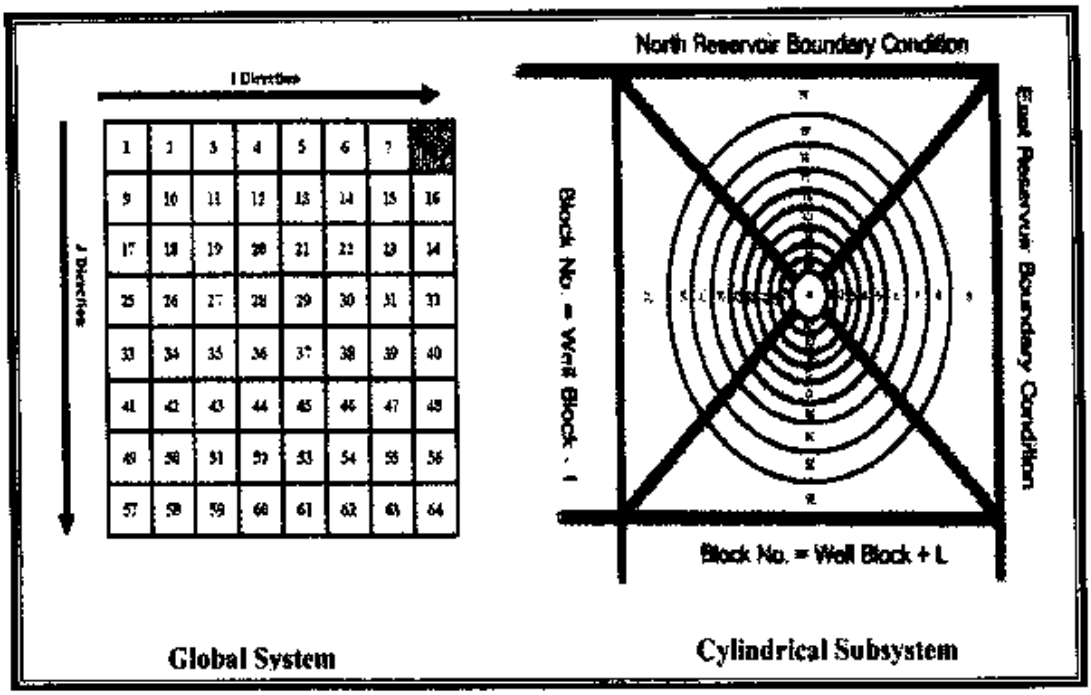

Figure (9) Numbering Scheme for Global and Cylindrical Systems.

Table (1) Basic Properties for case # 1.1

Basic Properties for Case # 1.1
Length = 5600 m width 5600 m Net Thickness 70 m Porosity = 19.0 % Horizontal Permeability = 175 md Initial Pressure 4377 Psi.
ΔX = 700 m ΔY = 700 m Well location in I = 8 , J = 1 No of Producer = 1
$rw = 0.1\ m$ $re = \{(\Delta x \cdot \Delta y - \pi r_{n-1}^2)/\pi\}^{1/2}\ m$ Logarithmic grid distribution N= number of grid in r direction = 9 M= number of grid in θ direction = 4

Table (2) Cylindrical Subsystem Results at 2500 Days (first run).

*** Elapsed Time = .34E+05 SEC.
*** DYNAMIC RADIAL
ACC. TIME = 2500.000 Day. DT.= .001000
Po (Psi.) LAYER 1
Acc. Oil Prod.= .81E+02 Acc. We= .00E+00 MSTB
I = 8 J = 1 P. avg.= 3907.5Psi.

J \ I								
2000	2000	2000	2000	2000	2000	2001	2072	3907
2000	2000	2000	2000	2000	2000	2001	2072	3907
2000	2000	2000	2000	2000	2000	2001	2072	3907
2000	2000	2000	2000	2000	2000	2001	2072	3907

Table (3) Cylindrical Subsystem Results at 2500 Days (second run).

*** Elapsed Time = .64E+05 SEC.
*** DYNAMIC RADIAL
ACC. TIME = 5000.000 Day. DT.= .000999
Po (Psi.) LAYER 1
Acc. Oil Prod.= .10E+03 Acc. We= .00E+00 MSTB
I = 8 J = 1 P. avg.= 3436.5Psi.

J \ I								
2000	2000	2000	2000	2000	2000	2000	2024	3436
2000	2000	2000	2000	2000	2000	2000	2024	3436
2000	2000	2000	2000	2000	2000	2000	2024	3436
2000	2000	2000	2000	2000	2000	2000	2024	3436